THE ASTRONOMICAL JOURNAL, 122:849–857, 2001 Augsut

SUPERNOVA REMNANTS IN THE SOUTHWESTERN PART OF THE SMALL MAGELLANIC CLOUD

JOHN R. DICKEL[1]
Department of Astronomy, University of Illinois at Urbana-Champaign, 1002 West Green Street, Urbana IL 61801; johnd@astro.uiuc.edu
ROSA M. WILLIAMS[2]
NASA Goddard Space Flight Center, Code 662, Greenbelt MD 20771; rosanina@milkyway.gsfc.nasa.gov
LYNN M. CARTER[3]
Department of Astronomy, University of Illinois at Urbana-Champaign, 1002 West Green Street, Urbana IL 61801; lcarter@astrosun.tn.cornell.edu
D. K. MILNE
Australia Telescope National Facility, Box 76, Epping, NSW 1710, Australia; Doug.Milne@atnf.csiro.au
ROBERT PETRE
NASA Goddard Space Flight Center, Code 666, Greenbelt MD 20771; rob@milkyway.gsfc.nasa.gov
AND
SHAUN W. AMY[4]
Australia Telescope National Facility, Box 76, Epping, NSW 1710, Australia; Shaun.Amy@atnf.csiro.au
Received 2001 January 19; accepted 2001 April 25

ABSTRACT

We have compared radio images from the Australia Telescope Compact Array and X-ray images from *ROSAT* of an area about 560 pc in diameter around the very extended emission nebula N19 on the southwestern edge of the bright ridge of the Small Magellanic Cloud. These data have allowed us to identify tentatively seven supernova remnants in this region. This number is large enough to suggest that the area has recently undergone some starburst activity. N19 itself appears to contain two overlapping supernova remnants within the extended H II region.

Key words: Magellanic Clouds — supernova remnants

1. INTRODUCTION

The southwestern area of the main ridge of the Small Magellanic Cloud (SMC) is an area of great stellar activity. It contains many emission nebulae, including the second-largest one in the SMC, LHα 115-N19 (Henize 1956), which extends over more than 100 pc. (In keeping with common practice, we shall hereafter designate this and other nebulae from the Henize (1956) catalog simply by the letter N followed by the catalog number.) As well as many emission nebulae, there are several supernova remnants (SNRs; e.g., Mathewson et al. 1984) and some stellar associations (Hodge 1985). To understand the implications of the activity in this region, we need to determine the nature of the various sources of radiation observed from X-ray through radio wavelengths. To date, the limited spatial resolution of the radio and X-ray telescopes and incomplete coverage of the optical emission have made it difficult to ascertain the relation among the observations in different wavelength regimes. The specific nature of several individual sources in that area remains unknown.

The largest emission nebula, N19, is certainly not the brightest optically, but parts of this complex do show bright X-ray (Inoue, Koyama, & Tanaka 1983) and radio (Mills et al. 1982) emission, plus strong [S II] line emission (Rosado, LeCoarer, & Georgelin 1994) and significant internal motions (Chu & Kennicutt 1988). These characteristics indicate the presence of one or more SNRs within N19. There also appear to be overlapping thermal and nonthermal components plus variable extinction in this complex.

Several other definite SNRs and H II regions lie within an area of about 0°.5 diameter ($\sim$500 pc) in this part of the SMC. A few of these objects have unusual properties. For example, the nebula N30 is very prominent at radio wavelengths (Turtle et al. 1998) but is not visible in X-rays, while SNR J0049.2−7314 is bright in X-rays (Inoue et al. 1983) but barely visible in the radio (Mathewson et al. 1984).

To understand these variations and improve our knowledge of all the objects in this region, we have observed a field around N19 with the Australia Telescope Compact Array (ATCA) at frequencies of 1.34 and 2.4 GHz with half-power beamwidths of $10 \times 5''$ (elliptical) and $4''.5$ (circular), respectively. These data were compared with the X-ray images and spectral data from the *ROSAT* Position Sensitive Proportional Counter (PSPC) survey of the SMC and supplementary data from the High Resolution Imager (HRI; Snowden 1999). The results have allowed us to distinguish between SNRs and H II regions in some cases, and we have compiled a list of seven proposed SNRs within the area.

In § 2, we describe the observations. The data are presented in § 3 and discussion follows in § 4.

2. EQUIPMENT AND OBSERVATIONS

The radio observations were conducted simultaneously at the two frequencies of 1.34 and 2.4 GHz using four different baseline configurations of the ATCA (ATCA 1992) for a total of 53 interferometer spacings between 31 and 6000 meters. After editing, imaging, and CLEANing, the resultant images were restored with Gaussian beam patterns. Because of editing, the beam response at 1.34 GHz was

[1] Visiting Astronomer at ASTRON, 7990AA Dwingeloo, Netherlands.
[2] NAS/NRC Postdoctoral Fellow.
[3] Current address: Department of Astronomy, Cornell University, 512 Space Sciences Building, Ithaca, NY 14853.
[4] Also at Department of Astrophysics, University of Sydney, Sydney NSW 2006, Australia.

elliptical so that image has been restored with a half-power beamwidth (HPBW) of 10″ × 5″ at P.A. 8°; the 2.4 GHz image was restored with a circular beamwidth of 4.″5. For the spectral index image, the 2.4 GHz image was convolved to the beam of the 1.34 GHz image.

Much strong interference was present in the data at 2.4 GHz. This interference required removal of large sections of the data set, which created noticeable distortion of the beam pattern and reduced sensitivity. At 1.34 GHz, only a modest number of data needed to be excised because of interference. The rms noise levels measured in clear areas of the final cleaned images were 0.1 mJy beam^{-1} at both frequencies. This value is higher than expected for the system sensitivity and undoubtedly arises from confusion noise of the many complex sources in the field interacting with the imperfect beam patterns. This conclusion is confirmed by the fact that the Stokes V (circularly polarized) image, which should contain no confusing signal, has an rms of only 0.033 mJy beam^{-1}, one-third of that found on the total intensity image.

The images were centered at R.A. = 00^{h}48^{m}00^s, decl. = −73°16′00″ (J2000.0). The field of view of the images shown in Figures 1*a* and 2 extends to the half-power point of the primary beam of each, and a correction for the decrease of sensitivity as a function of distance from the field center has been applied. The noise is therefore somewhat higher near the edges of the field. Figure 1*b* covers the area around J0051.9−7310, which lies outside the half-power field of view at 1.34 GHz and is very close to a strong radio point source. That part of the image is very noisy, and it was not possible to clean the point source very well on such a steep gradient in the response pattern. The image illustrates that we cannot detect the X-ray identified SNR at radio wavelengths to rather modest limits.

X-ray observations of this field using the *ROSAT* PSPC (data set rp500249) were retrieved from the *ROSAT* archive

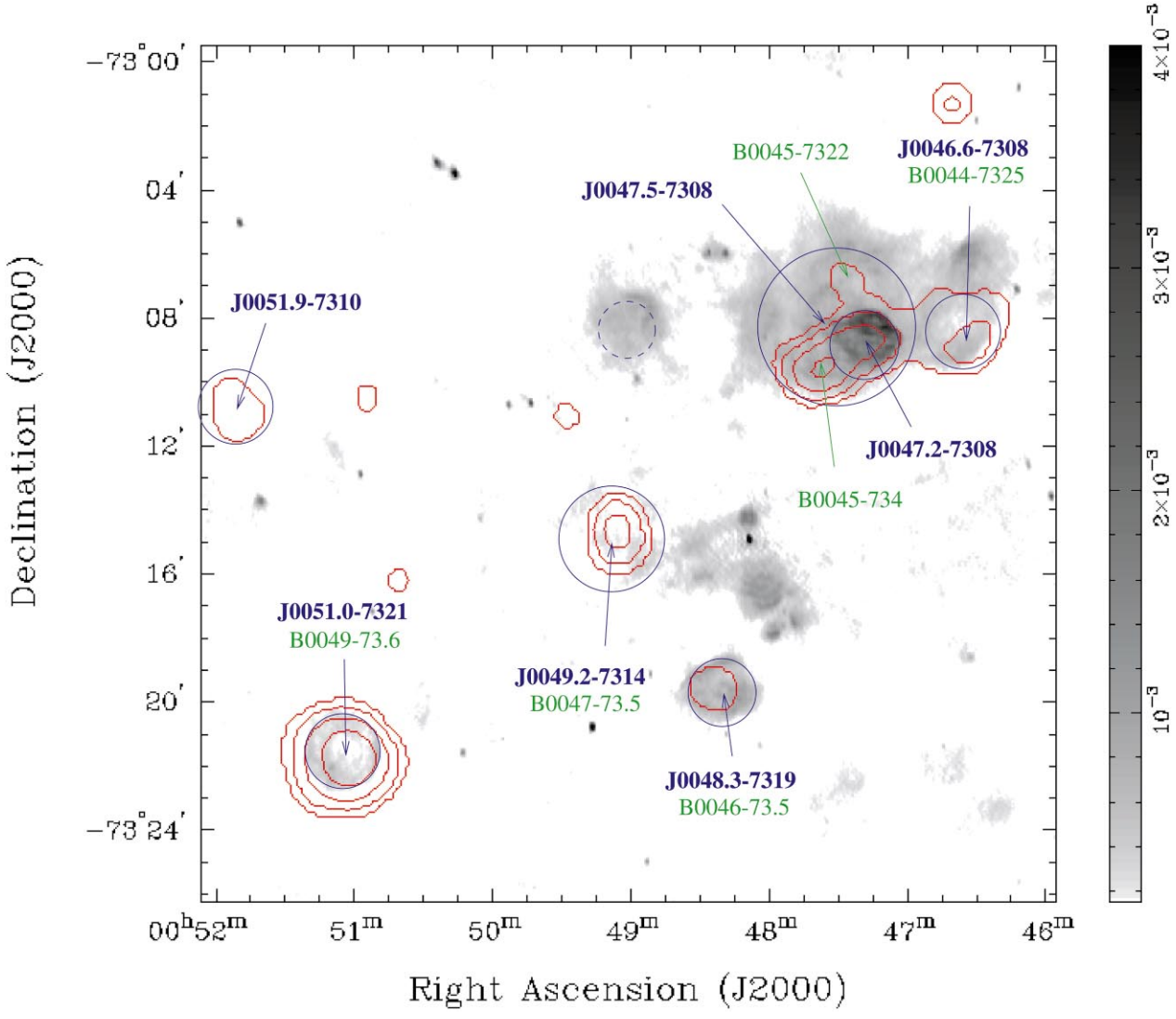

FIG. 1*a*

FIG. 1.—(*a*) Radio image of the southeastern end of the ridge of the SMC at a frequency of 1.34 GHz with superposed contours (*red*) of the *ROSAT* PSPC emission. The radio half-power beamwidth is 10″ × 5″ at P.A. 8°. The contours are 2, 4, 8, and 16 σ over the background on the X-ray image, assuming Poisson statistics. The B designations (*green*) are from Mathewson et al. (1984), citetr94, and citetw92. The J designations (*blue*) are from the current work. (*b*) Same as (*a*), but enlarged to show the region J0051.9 − 7310 with the radio background more prominently displayed. The contours are 1, 2, and 3 σ over the background on the X-ray image.

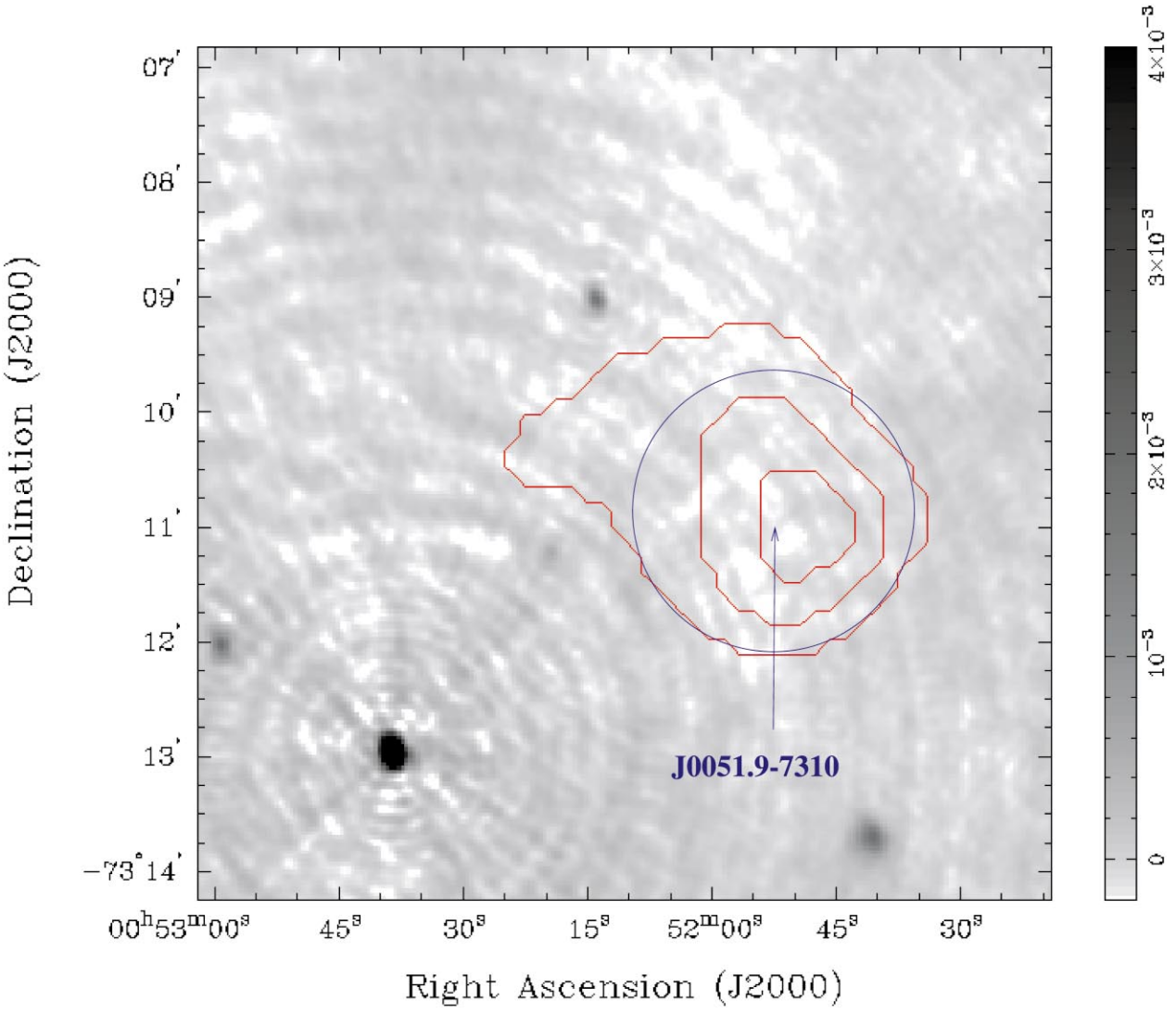

FIG. 1*b*

(Fig. 3*a*). The PSPC covers a spectral range from 0.1 to 2.4 keV, with an energy resolution of ~43% at 1 keV. It has a field of view 2° in diameter and an on-axis angular resolution of ~30″ (Pfeffermann et al. 1987). The observation was centered at R.A. = $00^h46^m41^s$, decl. = −73°12′36″ (J2000.0) and had a live-time duration of 18.6 ks.

Additional exposures using the *ROSAT* HRI (data sets rh400340, rh500136, and rh500419) were retrieved from the archive. A mosaic of these images, with a resolution of approximately 5″ pixel^{-1}, was formed using the Extended Source Analysis Software of Snowden (1995). This mosaic, shown in Figure 3*b*, was used to examine most of the region at somewhat higher resolution; however, because the HRI is less sensitive to diffuse emission, much of the fainter structure is lost.

3. RESULTS

3.1. *Morphology*

A gray scale of the 1.34 GHz radio image of this region of the SMC with superposed *ROSAT* PSPC contours is shown in Figure 1. Sources with J2000.0 coordinate designations represent definite or probable SNRs. Sources with B1950 coordinates had previously been identified as SNRs by Mathewson et al. (1984) or Rosado et al. (1994). Some of the source characteristics are given in Table 1. The source designations in Table 1 are given by the acronym MCRX, standing for Magellanic Cloud radio–X-ray source, followed by the truncated J2000.0 coordinates. Hereafter in the text we shall refer to the sources only by their coordinate designations. A 2.4 GHz image of the smaller area covered by its beam is shown in Figure 2. One SNR, MCRX J0051.0−7321 was outside the 22′ field at 2.4 GHz and is included only at 1.34 GHz. The X-ray images (*ROSAT* PSPC and HRI) of the region are shown in Figure 3.

N19, as cataloged by Henize (1956) encompasses an area of 5.′2 × 7.′0 centered near R.A. = $00^h47^m35^s$, decl. = −73°06′30″. The bright asymmetric ring at R.A. = $00^h47^m17^s$, decl. = −73°08′43″ on the western side of this complex is the brightest structure on the whole radio image, and it is also the area of brightest [S II] emission (Rosado et al. 1994). The brightest X-ray peak, however, is farther east, at R.A. = $00^h47^m36^s$, decl. = −73°09′40″, though the X-ray emission is bright over the entire southern part of N19. The Hα emission remains prominent well north of these features, indicating that N19 is indeed a complex of probably interacting SNRs and H II region components.

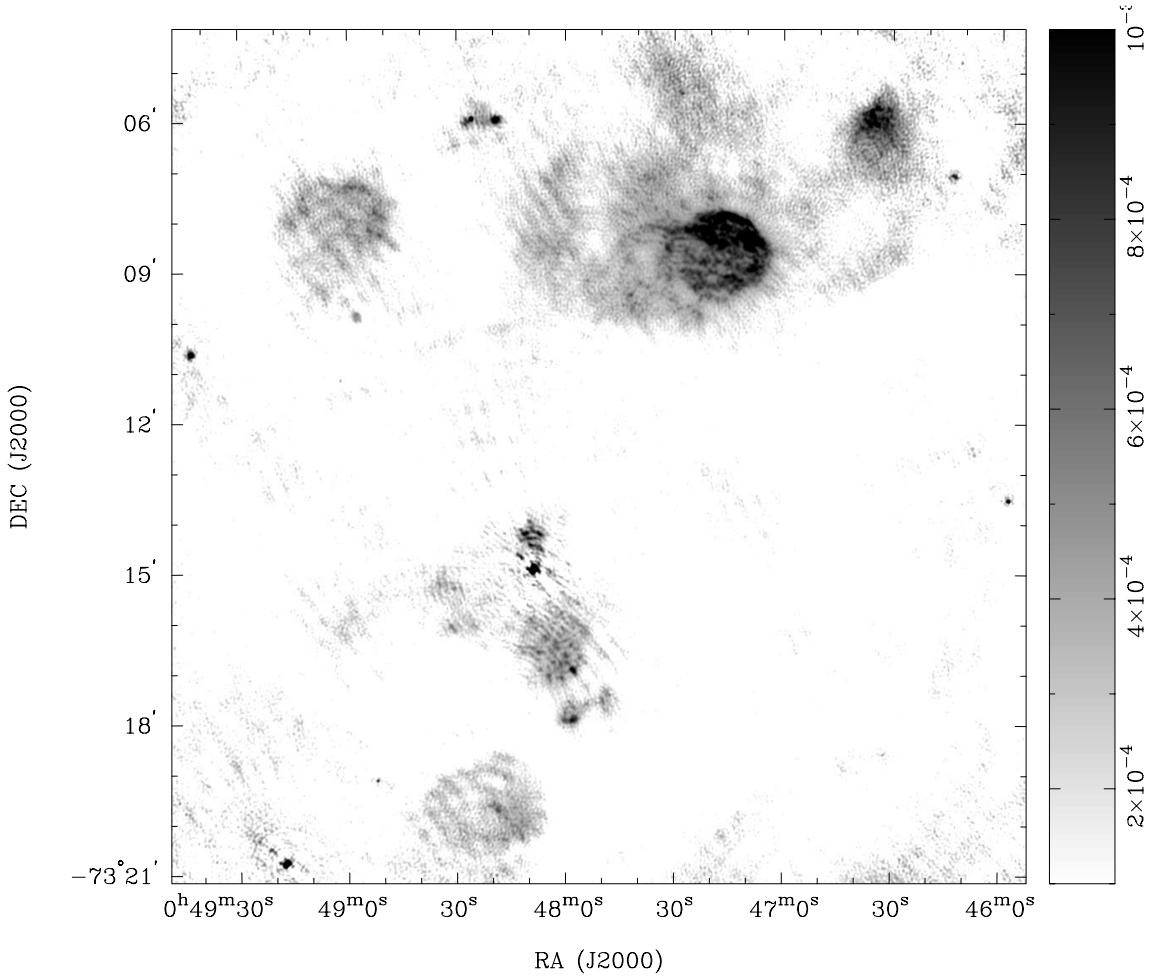

FIG. 2.—Radio image of a smaller area around the southeastern end of the ridge of the SMC at a frequency of 2.4 GHz. The half-power beamwidth is 4″.5.

The optical emission of N19 does not extend westward to cover the arc of radio and X-ray emission centered at R.A. = $00^h46^m38^s$, decl. = −73°08′24″, which we designate as a separate object, J0046.6−7308. The presence of both prominent radio and X-ray emission suggests that J0046.6−7308 is a definite SNR. The bright radio spot north of the latter object is a prominent H II region N12A. The optical emission from SNRs is often relatively faint and there could also be some extinction reducing the optical emission in the direction of the SNR.

Other obvious SNRs are J0048.3−7319, which contains N24, and also J0051.0−7321. The former source is relatively faint in X-rays. The latter source is neither a Henize (1956) nor DEM (Davies, Elliott, & Meaburn 1976) nebula although the image in the latter paper does appear to show a faint unlisted Hα emission feature at the correct position,

TABLE 1

SNRs IN THE VICINITY OF N19 IN THE SMC

MCRX J	R.A (J2000.0)	Decl. (J2000.0).	DIAMETER (pc)	S_f (mJy) 1.34 GHz	2.4 GHz	1 GHz	SP. INDEX	$\Sigma_{1\ \mathrm{GHz}}$ (10^{-21} W m^{-2} Hz^{-1} sr^{-1})	$L_{\mathrm{X\text{-}ray}}$ (10^{34} ergs s^{-1})
0046.6−7308.....	00 46 38	−73 08 24	43	69	49	82	−0.6	1.7	7.7
0047.2−7308.....	00 47 17	−73 08 43	31	250	225	265	−0.2	10.0	6.8
0047.5−7308.....	00 47 30	−73 08 00	80	400	300	460	−0.5	2.8	11.0
0048.3−7319.....	00 48 22	−73 19 36	35	100	58	130	−0.9	4.0	1.9
0049.2−7314.....	00 49 12	−73 14 51	53	28	[a]	(30)	...	0.4	6.1
0051.0−7321.....	00 51 05	−73 21 39	40	42	[b]	(50)	...	1.2	42
0051.9−7310.....	00 51 54	−73 10 24	...	[c]	...	...	...	...	5.1

NOTE.—Units of right ascension are hours, minutes, and seconds, and units of declination are degrees, arcminutes, and arcseconds.

[a] Too faint to be measured at 2.4 GHz.

[b] Outside field of view at 2.4 GHz.

[c] Undetectable on edge of field of view.

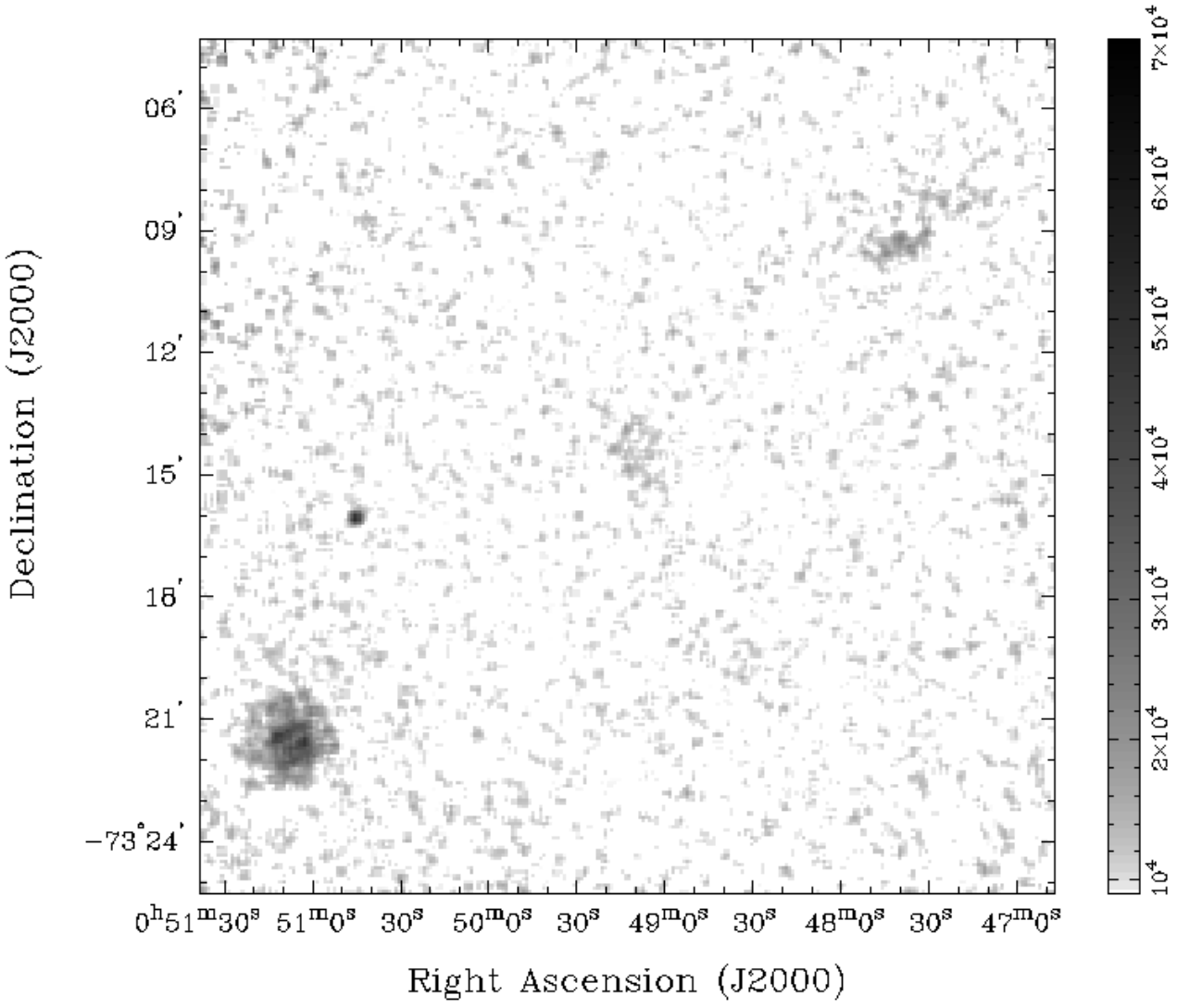

FIG. 3*a*

FIG. 3.—X-ray images from *ROSAT* (*a*) HRI, binned to 5″ pixel^{-1}, and (*b*) PSPC, binned to 15″ pixel^{-1}. Both are convolved with a boxcar adaptive filter.

just at the northeastern edge of DEM S53. The X-ray image of J0051.0−7321 is well defined, showing an uneven distribution of X-ray emission over the face of the remnant. J0049.2−7314 is also a definite SNR (Mathewson et al. 1984), with faint shell-like X-ray emission, although its radio surface brightness is very low and it is only marginally detected with the relatively high angular resolution of the present observations.

The object J0051.9−7310 shows an X-ray hardness ratio similar to all the other SNRs, but it lies on the edge of the field of view of the 1.34 GHz radio image and is undetected at a 3 rms surface brightness of less than 0.4 mJy beam^{-1}. This limit is near that found for several detected SNRs so we cannot exclude the presence of a radio remnant at that position and conclude that the object is an SNR.

The one-contour X-ray source at R.A. = $00^h50^m40^s$, decl. = −73°16′15″ is a hard X-ray pulsing Be star with a period of 323 s (Imanishi et al. 1999). To identify the remaining two-contour X-ray source, at R.A. = $00^h46^m40^s$, decl. = −73°01′15″, we looked in the SMC X-ray catalog of Kahabka et al. (1999). The closest source to our object is RXJ 0046.5−7300 (R.A. = $00^h46^m35^s.3$, decl. = −73°00′59″), a probable foreground star. This identification is strengthened by the low hardness ratio of this source in our observations. Another 2 σ X-ray source, just outside the field shown, at R.A. = $00^h45^m10^s$, decl. = −73°04′20″, can be identified with RXJ 0045.1−7303 ($00^h45^m08^s.5$, −73°03′56″), a probable background source (active galactic nucleus, quasar, etc.). Both *ROSAT* sources are within the positional error given by Kahabka et al. (1999). All the other extended radio features on the images have optical counterparts and appear to be H II regions.

3.2. *Spectral Properties*

3.2.1. *Radio Spectral Indices*

The data at the two radio frequencies can be combined to form a spectral index map of the region. This map should help to distinguish the thermal and nonthermal components. Figure 4 is a gray-scale image of the spectral index with contours of the 1.34 GHz intensity. The display is cut off wherever either of the input images was less than 2 times the rms noise level. We adopt the convention for the spectral index, α, of $S_f \propto f^{\alpha}$, where S is the surface brightness and f is the frequency; thus, negative values are nonthermal

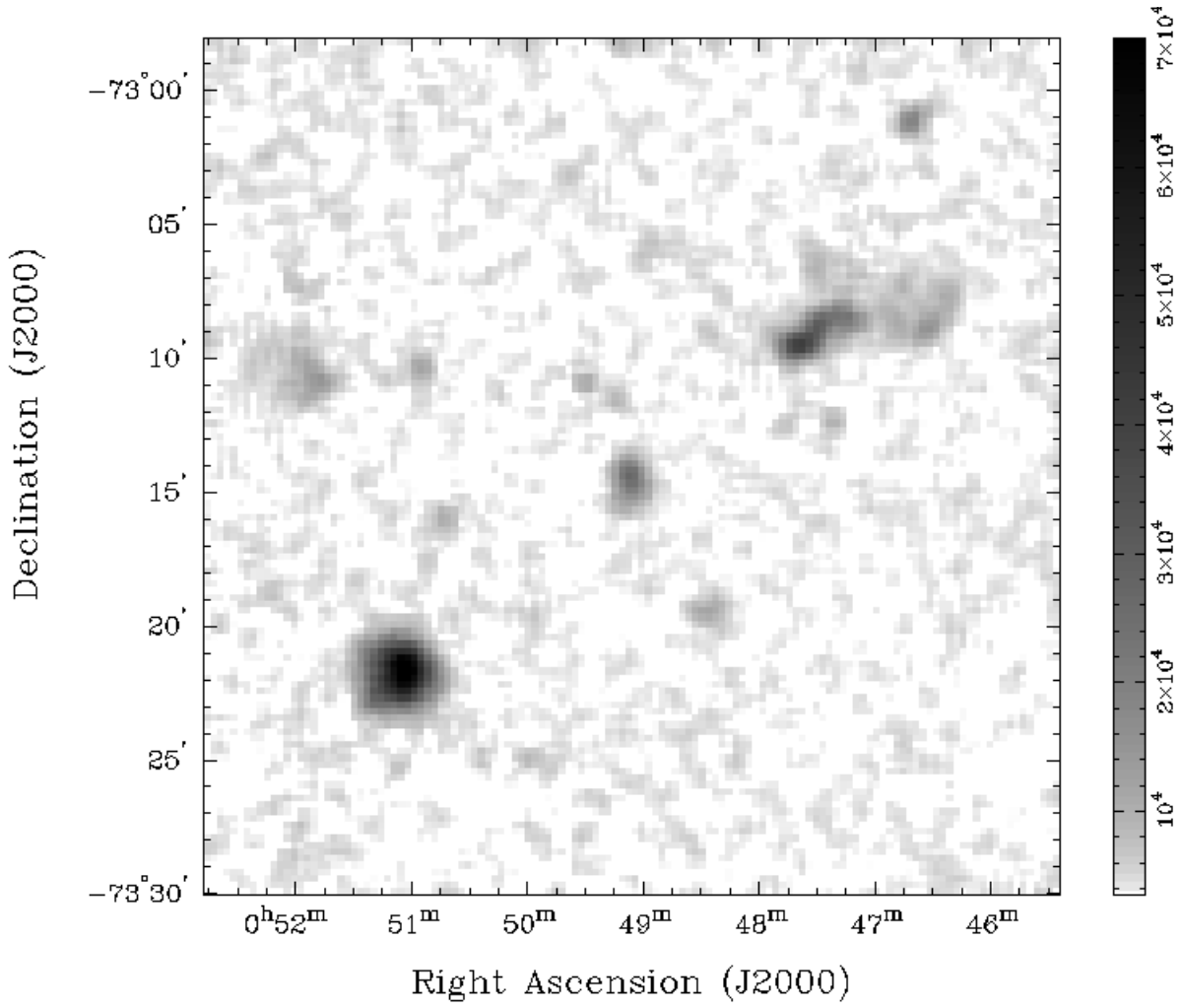

FIG. 3*b*

or lighter on this image. Because the ratio of the two frequencies is only 1.8 and the background is very noisy and near the brightness levels of most of the sources, this spectral index map is of only limited value. However, some trends can be seen.

J0048.3−7319 is confirmed as a nonthermal SNR. The entire southern region of N19, encompassing the definite SNR J0047.2−7308 and the proposed SNR candidate J0047.5−7308, has a relatively steep radio spectrum, as well as bright X-ray emission. Although the arc J0046.6−7308, just west of N19, is faint, the few points where the spectrum can be determined also show nonthermal values. By contrast, at least the brightest (and thus most reliable) part of N12A to the north, at R.A. = $00^h46^m35^s$, decl. = $-73°05'45''$, appears to be thermal.

We have fitted Gaussians to the emission from the bright source near the center of the image at R.A. = $00^h48^m08^s.53$, decl. = $-73°14'54''.3$ (N26 in Henize's 1956 list). Within the errors of the fits at both frequencies, it is a point source with flux densities of 12 and 10 mJy at 1.34 and 2.4 GHz, respectively. These values give a spectral index of −0.3, similar to that seen on the spectral index image. The extended source to the north plus the three to the south that are aligned with the point source all appear to have similar outlines in the optical and radio but no X-ray emission. Their radio spectral indices are relatively steep. The point source has been detected in CO with SEST (Israel et al. 1993). Hα kinematics of this region reported by LeCoarer et al. (1993) shows a normal velocity field without any evidence of violent motions but with a strong continuum. This velocity pattern would support the lack of SNRs and X-ray emission but not explain an apparent nonthermal component to the radio emission. The full nature of this entire complex remains undetermined. It might contain some background features, as well as H II regions.

The bright Hα feature (Fig. 1*a*) marked by the dashed circle centered at R.A. = $00^h49^m02^s$, decl. = $-73°08'15''$ has an uncertain radio spectrum, which is probably caused by background variations. It has no detectable X-ray emission and only weak [S II] emission, so we consider it to be an H II region.

3.2.2. *X-Ray Hardness Ratios*

Separate soft (0.25 keV) and hard (1.25 keV) PSPC X-ray images of this area of the SMC show some differences between the sources. The only significant features seen on the soft X-ray map are J0051.0−7321, probably J0051.9−7310, and the two-contour source in the north at R.A. = $00^h46^m40^s$, decl. = $-73°01'15''$. The first two are

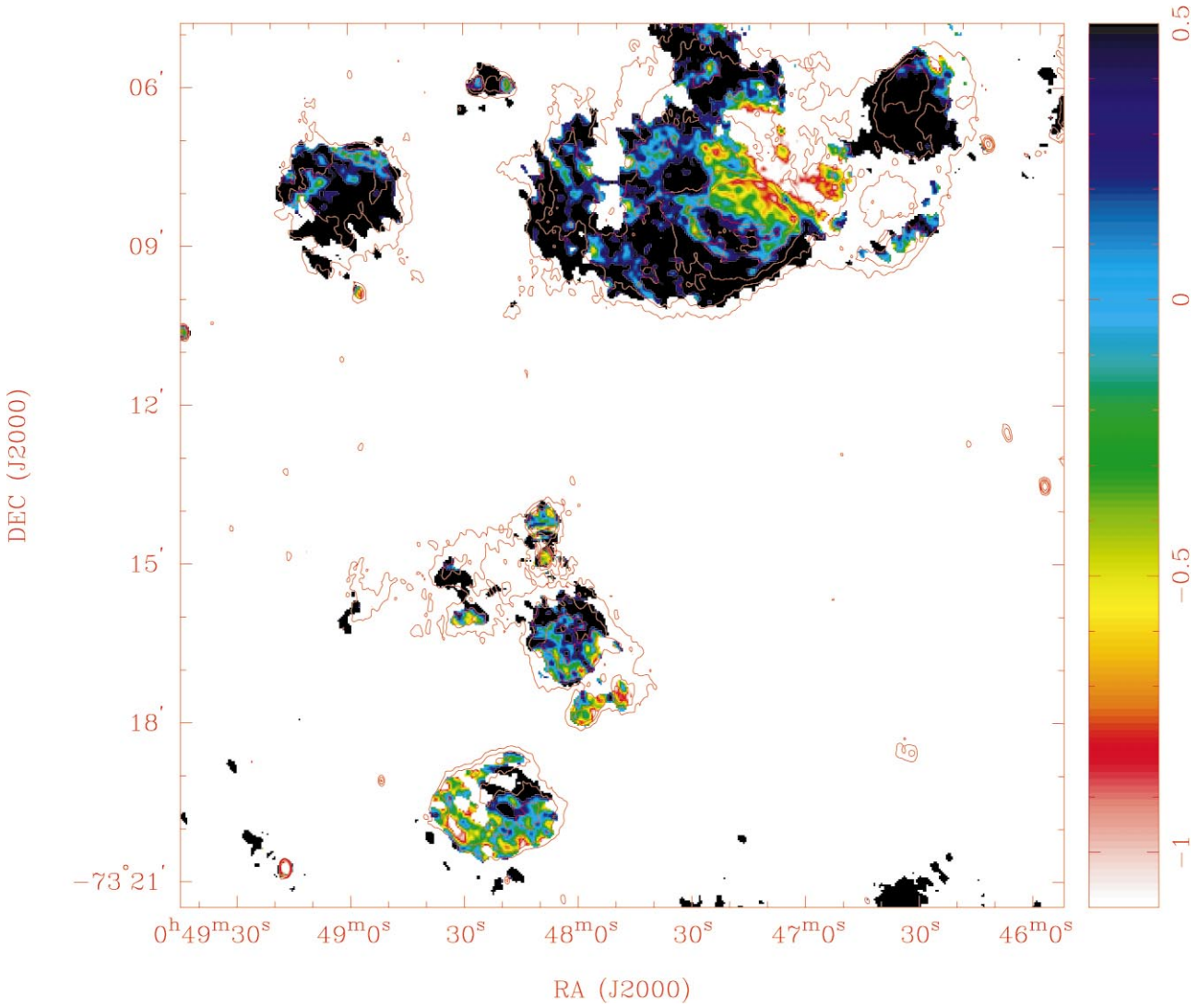

FIG. 4.—Radio spectral index image of the southeastern end of the ridge of the SMC with contours of the intensity of the 1.34 GHz image. The contour levels are 0.3, 0.6, 1.0, and 2.0 mJy beam^{-1}. Wherever there is no color, the emission at one of the two observing frequencies was too faint to be measured accurately.

also very bright in the hard band and appear to have hard spectra. The third source is very faint in the hard band and has a soft spectrum. In the hard band we find bright emission from the entire southern part of N19 and the separate SNRs J0048.3−7319, J0049.1−7314, and J0046.6−7308. An actual hardness ratio map appears as a noisier version of the hard-band image because of the low signal-to-noise ratio on the soft-band image.

3.2.3. *X-Ray Spectral Fits*

Using the XSPEC spectral analysis program, we analyzed the *ROSAT* PSPC spectral data from these remnants. A number of trials were run for each SNR, in which models of thermal bremsstrahlung, a power law indicating possible nonthermal emission, and thermal plasma emission were compared with the data. The thermal plasma models used in these fits include the formulation of Mewe and Kaastra with Fe L calculations by Liedahl (Mewe, Kaastra, & Leidahl 1995, hereafter MeKaL; Phillips et al. 1999), the formulation of Raymond and Smith (Raymond & Smith 1977, hereafter RS; Brickhouse, Raymond, & Smith 1995), and a simple nonequilibrium ionization (NEI) plasma model. The X-ray luminosities for these SNRs over the *ROSAT* band (0.1–2.4 keV) are given in Table 1, while spectral model fits are summarized in Table 2.

For the X-ray bright SNR J0047.5−7308 in N19 and the isolated objects J0049.2−7314 and J0051.0−7321, the thermal bremsstrahlung and power-law models could be ruled out at the 90% confidence level or above. However, for the fainter sources J0046.6−7308, J0047.2−7308, J0048.3−7319, and J0051.9−7310 the number of counts available in the integration is insufficient to constrain the models to this degree.

For J0047.5−7308 and J0049.2−7314 the best fits to the data were thermal models in which all abundances but iron were fixed at 0.2 times the solar abundance, typical of the SMC (Russel & Dopita 1992), while the iron abundance was allowed to vary freely. In both cases the resulting iron abundances were higher than the typical SMC abundances. Though the values of the parameters are uncertain by a factor of 2, it seems probable that both of these remnants have significant iron enhancement.

For the bright SNR on the southeastern corner of the field, J0051.0−7321, on the other hand, an NEI plasma

TABLE 2

X-Ray Spectral Fits for SNRs in the Vicinity of N19

MCRX J	Best-Fit Model[a]	χ^2/dof	kT (keV)	N_H (10^{22} cm^{-2})	Other Notes
0046.6−7308.....	MeKaL	18/17	0.52	0.064	Bremss, power not excluded at 90% confidence
0047.2−7308.....	MeKaL	18/17	0.85	0.25	Bremss, power not excluded at 90% confidence
0047.5−7308.....	MeKaL	14/17	0.39	0.69	Fe enhanced (∼0.6 solar abundance)
0048.3−7319.....	MeKaL	12/17	0.86	0.019	Bremss, power not excluded at 90% confidence
0049.2−7314.....	RS	14/16	0.81	0.033	Fe enhanced (∼2.4 solar abundance)
0051.0−7321.....	NEI	9/16	0.36	0.050	Fe depleted (∼0.1 solar abundance)
0051.9−7310.....	Bremss	12/17	0.40	0.34	Plasma, power not excluded at 90% confidence

[a] XSPEC models used include Mewe et al. thermal plasma (MeKaL), Raymond-Smith thermal plasma (RS), plasma with nonequilibrium ionization (NEI), power law (power), and bremsstrahlung (bremss).

model with abundances other than iron fixed at 0.2 solar and iron free to vary gave the best fit. In this case, the fitted abundance for iron was below the fixed abundances of the other elements with a value of 0.1 ± 0.8 solar to 90% confidence. It should be noted that similar results could be obtained for models assuming collisional equilibrium; the number of counts in the X-ray spectra may not be sufficient to constrain the ionization conditions for this remnant.

For J0046.6−7308, J0047.2−7308, J0048.3−7319, and J0051.9−7310 the results shown in Table 2 are the best of several statistically allowable model fits. In the cases of J0046.6−7308, J0047.2−7308, and J0048.3−7319 a simple thermal plasma model with fixed abundances provided the best fit, while for J0051.9−7310 a thermal bremsstrahlung model provided the best fit. Because of the large uncertainties involved, however, these fits must be regarded as tentative.

3.3. *Radio Polarization*

We find no polarized signal above 0.12 mJy beam^{-1} at 2.4 GHz and about 0.1 mJy beam^{-1} at 1.34 GHz, although there appear to be some residual artifacts in the polarized image at 1.34 GHz. These values give upper limits to the polarized fractions toward J0047.2−7308 of 0.12 and 0.04 at 2.4 and 1.34 GHz, respectively, and higher toward the other sources. Values below this are quite common in young, bright SNRs but the data do not allow us to determine any information on the magnetic fields present in these objects.

4. DISCUSSION

Clearly N19 contains at least one SNR, but the variety of structures seen in the different wavelength bands has yet to reveal a consistent picture. The brightest asymmetric ring structure on the radio image, about 2′ in diameter, centered within N19 at R.A. = $00^h47^m17^s$, decl. = −73°08′43″, looks like a distinct SNR, but in X-rays it appears to be more of an extension from the brightest point in the southeast curving around to a northerly arc. From the [S II]/Hα ratio, Rosado et al. (1994) suggest an elliptical remnant of axial ratio 1.7 with the major axis pointing southeast-northwest; the southern edge extends down to the southern edge of the X-ray contours but not as far east as the brightest X-ray emission. Rosado et al. (1994) also fitted another ellipse to a high [S II]/Hα partial ring just north of the previous candidate; it overlaps the increased radio and X-ray emissions in that area that do not fully coincide with one another. There are some other bright [S II] features in N19 about which Rosado et al. (1994) do not comment. One slit spectrum nearly across the center of the bright radio ring in an east-west direction (Chu and Kennicutt 1988) and Fabry-Perot observations by Rosado et al. (1994) over their selected SNRs all show full-width zero-intensity line widths of about 350 km s^{-1} in both Hα and [S II].

Considering all these data together, we tentatively assign the bright radio ring as one SNR with the designation J0047.2−7308. It is superposed on another with an approximately circular outline of diameter 5′ (80 pc) with the designation J0047.5−7308. The northern part of N19 is most likely an H II region that probably extends down to encompass the region of the two SNRs.

With these identifications, we end up with a total of seven probable SNRs within an area of about 35′ (560 pc) on a side. This is a large number of SNRs in a small volume. Assuming a depth along the line of sight also equal to 560 pc, we find one SNR per 25×10^6 pc^3, or a mean separation between SNRs of about 400 pc. The same density in the Milky Way would give about 3×10^4 remnants in our Galaxy, about 150 times as many as are known.[5] We know of no such densely packed region of SNRs in the Milky Way.

We note that the distribution of extended radio sources in the SMC is very irregular, with this area appearing to be one of the most populous (Turtle et al. 1998). There is also an 87.6 ms X-ray pulsar, AX J0043−736, just outside our field of view (Yokogawa & Koyama 2000). Sixteen stellar associations are present in that same area (Hodge 1985), but only two are coincident with features discussed above—N19 and one encompassing the point source N26 and its peculiar surrounding features. None of these associations are very rich but together they can be significant. While N19 is faint, it is over 100 pc across and the other H II regions combined also cover a rather large area. In addition, there is a large H I bubble with a radius of 157 pc centered at R.A. = $00^h47^m42^s$, decl. = −73°10′57″ (Staveley-Smith et al. 1997). Its large size and reasonably high expansion velocity of 15.1 km s^{-1} require a substantial wind luminosity. Thus, there are several consistent lines of evidence suggesting at least modest starburst activity in this region and a possible low density for the overall medium within the shell. A complete survey of the SMC is needed to determine whether this rate is a global property of the galaxy or a more localized phenomenon.

The X-ray results for the three SNRs bright enough for reasonable spectral modeling are intriguing. It has been

[5] See http://www.mrao.cam.ac.uk/surveys/snrs/.

argued (Nisiuchi et al. 2001) that the excess of emission around 1 keV, interpreted as an overabundance of iron, may suggest that the progenitor of the SNR origin was a Type Ia supernova. However, both remnants that show an apparent iron excess, J0047.5−7308 and J0049.2−7314, are within this region of apparent recent active star formation. J0047.5−7308 is actually within the H II region N19. The surroundings, then, are more indicative of a Type II origin. Lest this effect be thought a function of the SNR luminosity, we have the counterexample provided by J0051.0−7321, which appears *under*abundant in iron.

This dilemma may be addressed by noting the relatively slight iron overabundance in J0047.5−7308 and its confusion with other SNRs in the N19 region. It is possible that some of the emission attributed to J0047.5−7308 could, for example, be background emission from J0046.6−7308 serving to confuse the issue. We might then suggest that the relatively isolated remnant J0049.2−7314 was the result of a Type Ia supernova while the other isolated object, J0051.0−7321, was the result of a Type II supernova. However, the uncertainties of the model fits are such that we cannot place great confidence in this conclusion.

In summary, combined radio and X-ray observations of an area about 500 pc on a side around N19 in the SMC indicate the presence of seven shell supernova remnants. So large a number in a relatively small area suggests a modest starburst although there is no particularly significant core to this activity. The individual remnants are all reasonably large, indicating generally low-density surroundings. At least one object may show possible iron enhancement, which would suggest an origin in a Type Ia supernova and little mixing with swept-up material from the surroundings. Collectively, the remnants show a significant range in both radio and X-ray luminosities and other properties but with no correlations between any of the measured properties. Except for an apparently high concentration in a small volume, they appear to be similar to a random sample of middle-aged SNRs in the Milky Way.

Martin Guerrero kindly provided [S II]/Hα ratios for some of the observed radio sources in advance of publication. We thank M. Rosado for accurate coordinates of her emission-line images and helpful referee comments. R. M. W. acknowledges the support of the National Research Council. J. R. D. acknowledges a Visitor's Fellowship from the Netherlands Organization for Scientific Research during his stay at ASTRON. The ATCA is part of the Australia Telescope, which is funded by the Commonwealth of Australia for operation as a national facility managed by the CSIRO.

REFERENCES

ATCA. 1992, J. Electr. Electron. Eng. Australia, 12, 103
Brickhouse, N. S., Raymond, J. C., & Smith, B. W. 1995, ApJS, 97, 551
Chu, Y.-H., & Kennicutt, R. C. 1988, AJ, 95, 1111
Davies, R. D., Elliott, K. H., & Meaburn, J. 1976, MmRAS, 81, 89
Henize, K. G. 1956, ApJS, 2, 315
Hodge, P. W. 1985, PASP, 97, 530
Imanishi, K., Yokogawa, J., Tsuimoto, M., & Koyama, K. 1999, PASJ, 51, L15
Inoue, H., Koyama, K., & Tanaka, Y. 1983, in IAU Symp. 101, Supernova Remnants and Their X-Ray Emission, ed. P. Gorenstein & J. Danziger (Dordrecht: Reidel), 353
Israel, F. P., et al. 1993, A&A, 276, 25
Kahabka, P., Pietsch, W., Filipovic, M. D., & Haberl, F. 1999, A&AS, 136, 81
LeCoarer, E., Rosado, M., Goergelin, Y., Viale, A., & Goldes, G. 1993, A&A, 280, 365
Mathewson, D. S., Ford, V. L., Dopita, M. A., Touhy, I. R., Mills, B. Y., & Turtle, A. J. 1984, ApJS, 55, 189
Mewe, R., Kaastra, J. S., & Liedahl, D. A. 1995, Legacy, No. 6, 16
Mills, B. Y., Little, A. G., Durdin, J. M., & Kesteven, M. J. 1982, MNRAS, 200, 1017
Nisiuchi, M., Yokogawa, J., Koyama, K., & Hughes, J. P. 2001, PASJ, 53, 99
Pfeffermann, E., et al. 1987, Proc. SPIE, 733, 519
Phillips, K. H. J., Mewe, R., Harra-Murnion, L. K., Kaastra, J. S., Beierdorfer, P., Brown, G. V., & Liedahl, D. A. 1999, A&AS, 138, 381 (MeKaL)
Raymond, J. C., & Smith, B. W. 1977, ApJS, 35, 419 (RS)
Rosado, M., LeCoarer, E., & Georgelin, Y. P. 1994, A&A, 286, 231
Russel, S. C., & Dopita, M. A. 1992, ApJ, 384, 508
Snowden, S. 1995, Cookbook for Analysis Procedures for *ROSAT* XRT/PSPC Observations of Extended Objects and the Diffuse Background (Greenbelt, MD: GSFC)
———. 1999, in IAU Symp. 190, New Views of the Magellanic Clouds, ed. Y.-H. Chu, N. Suntzeff, J. Hesser, & D. Bohlender (San Francisco: ASP), 32
Staveley-Smith, L., Sault, R., Hatzidimitriou, D., Kesteven, M., & McConnell, D. 1997, MNRAS, 289, 225
Turtle, A., J., Ye, T., Amy, S. W., & Nicholls, J. 1998, Publ. Astron. Soc. Australia, 15, 280
Yokogawa, J., & Koyama, K. 2000, IAU Circ. 7361